Mean Flowfields in Axisymmetric Combustor Geometries with Swirl

D.L. Rhode* and D.G. Lilley†
Oklahoma State University, Stillwater, Oklahoma
and
D.K. McLaughlin‡
Dynamics Technology, Inc., Torrance, California

A swirling nonreacting flow enters a larger chamber via a sudden or gradual expansion. Six flowfield configurations are investigated with side-wall angles $\alpha = 90$ and 45 deg and swirl vane angles $\phi = 0$, 38, and 45 deg. Photography of neutrally buoyant helium-filled soap bubbles, tufts, and injected smoke helps to characterize the time-mean streamlines, recirculation zones, and regions of highly turbulent flow. From the photographic evidence, it is found that central recirculation zones occur for the swirling flow cases investigated, after which a relatively narrow precessing vortex core exists near the axis. Five-hole pitot probe pressure measurements allow the determination of time-mean velocities u, v, and w. At the inlet, the radial velocity profiles exhibit strong nonuniformity. The time-mean velocity measurements presented here constitute a seriously needed data base for the validation of computer prediction codes and the development of turbulence models for their simulation.

Nomenclature

D	= test section diameter
d	= inlet nozzle diameter
k	= kinetic energy of turbulence
p	= time-mean pressure
R	= radius of test chamber
Re	= Reynolds number
u,v,w	= time-mean velocity (in x,r,θ direction, respectively)
V	= time-mean vector velocity magnitude
x,r,θ	= axial, radial, azimuthal cylindrical polar coordinates, respectively
α	= side-wall expansion angle
β	= yaw angle of flow = $\tan^{-1}(w/u)$
δ	= pitch angle of flow = $\tan^{-1}[v/(u^2+w^2)^{1/2}]$
ϵ	= turbulence energy dissipation rate
ρ	= time-mean density
ϕ	= swirl vane angle = $\tan^{-1}(w_0/u_0)$

Subscripts

d	= based on inlet nozzle diameter
p	= based on probe tip diameter
0	= value at inlet to flowfield

I. Introduction

IN gas turbine and ramjet combustion chamber development, designers are aided by both experimental and theoretical studies.[1] The present research work is concerned with such complementary studies.[2-4] The problem being investigated is concerned with steady turbulent flow in axisymmetric geometries under low speed and nonreacting conditions—a study area which is fundamental to combustor modeling. The particular problem discussed in this paper is the flow in a round pipe entering an expansion into another round pipe as illustrated in Fig. 1. The incoming flow may possess a swirl component of velocity via passage through swirl vanes at angle ϕ from the axial direction, and the side wall may slope at an angle α, also from the axial direction. The resulting flowfield domain may possess a central toroidal recirculation zone in the middle of the region on the axis, in addition to the possibility of a corner recirculation zone near the upper corner provoked by the rather sudden enlargement of the cross-sectional area. Of vital importance is the characterization of flows of this type in terms of the effects of side-wall angle α, degree of swirl ϕ, turbulence intensity of the inlet stream, and expansion ratio D/d on the resulting flowfield in terms of its time-mean and turbulence quantities. Such problems have received little attention, although they are fundamental to the physical processes occurring in aircraft combustors.

A systematic parametric investigation is being undertaken on the effect of side-wall angle α and a swirl vane angle ϕ on the resulting flowfield produced. The goals of the ongoing study involve comparison of predictions with experimental turbulent flow measurements so as to assist in evaluating turbulence models and improving the final predictive capability. This paper focuses on the experimental study, with identification of recirculation regions from flow visualization and mean velocity measurements using a five-hole pitot probe, thus providing a useful data base for the later turbulence model development aspects of the study.

II. Experimental Approach

A. Previous Studies

There have been several experiments performed with nonreacting flows in expansion geometries that have been reported in the literature, examples of which are contained in Refs. 5,8. References 5-7 also include flowfield predictions, made with versions of the TEACH-T computer program.[9] These experiments include time-mean velocity measurements (with hot-wire and pitot probes and laser Doppler anemometry), turbulence measurements (with hot-wires and laser anemometers) and flow visualization. The majority of the earlier measurements were made in nonswirling flows; however, some noteworthy experiments have been made in swirling confined jets.[5,8] Direct comparison between the results of the cited experiments and the present experimental

Presented as Paper 82-0177 at the AIAA 20th Aerospace Sciences Meeting, Orlando, Fla., Jan. 11-14, 1982; submitted Jan. 22, 1982; revision received June 21, 1982.

*Graduate Student, School of Mechanical and Aerospace Engineering. At present: Assistant Professor, Department of Mechanical Engineering, Texas A&M University, College Station, Texas.

†Professor, School of Mechanical and Aerospace Engineering. Associate Fellow AIAA.

‡Group Manager. Member AIAA.

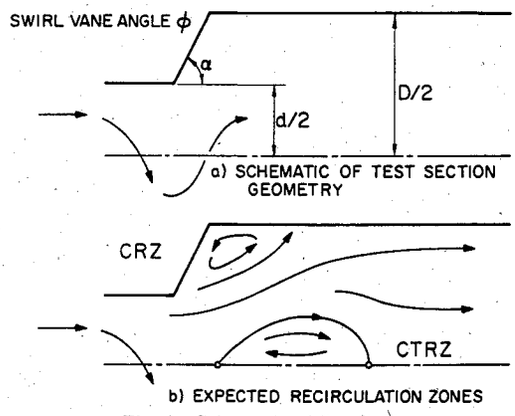

Fig. 1 Schematic of flowfield.

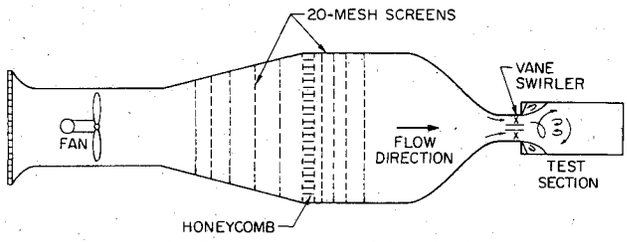

Fig. 2 Schematic of overall flow facility.

results is generally not possible because of differences in geometry. However, in the nonswirling jet, comparisons were possible with experiments of Chaturvedi,[8] who measured time-mean and turbulent flow quantities downstream of a sudden expansion of diameter ratio $D/d=2$ and various expansion side-wall angles α.

B. Test Facility

The present experiments have been conducted in the confined jet facility shown schematically in Fig. 2. The facility has an axial flow fan whose speed can be changed by altering the varidrive mechanism. Numerous fine screens and straws produce flow in the settling chamber of relatively low turbulence intensity. The contraction section leading to the test section has been designed by the method of Morel[10] to produce a minimum adverse pressure gradient on the boundary layer and thus avoid unsteady problems associated with local separation regions.

The test section consists of a swirl vane assembly and an idealized combustion chamber model. The swirl vane assembly contains ten vanes which are individually adjustable for any vane angle ϕ. The pitch/chord ratio of 1 provides good turning efficiency. The hub is located at the center of the swirler with a streamlined nose facing upstream. The downstream end is simply a flat face, simulating the geometric shape of a typical fuel spray nozzle.

The idealized combustion chamber model is composed of an expansion block and a long plexiglass tube. The expansion block is a 30-cm-diam disk with a 15-cm-diam hole centered on its axis through which the air entering the model flows smoothly. The downstream face of the expansion block has been shaped to provide the desired flow expansion angle α which is shown in Fig. 1. There are currently three interchangeable expansion blocks and the appropriate choice gives $\alpha=90$, 70, or 45 deg.

There are no film-cooling holes or dilution-air holes in the test facility, and the chamber wall consists of a straight pipe. The inside diameter of the pipe is 30 cm and the length is approximately 125 cm. The substantial size of the test model provides excellent resolution for five-hole pitot probe measurements and flow visualization photography.

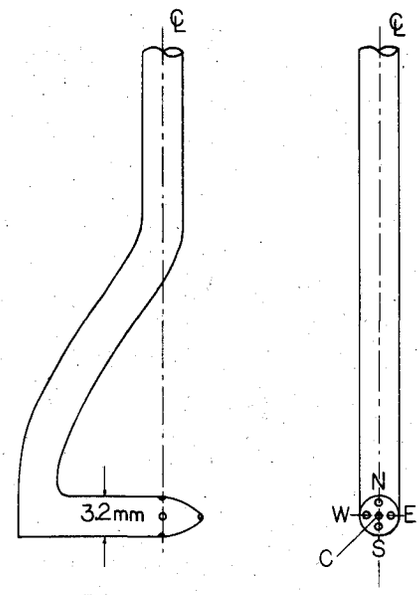

Fig. 3 Five-hole pitot probe.

C. Flow Visualization Techniques

A slide projector, located downstream of the test facility, served as the light source. A vertical sheet of light 4 cm thick was produced to illuminate the rx plane of the flow pattern. This was provided by using a slide which is opaque except for a thin slit cut out for light passage to the test section. Tri-X Pan, a very light-sensitive photographic film rated at ASA 400, along with a large camera aperture of f 2.0, was employed in order to obtain photographs of acceptable contrast. Moreover, the film was substantially overdeveloped to compensate for underexposure; this is equivalent to using an extremely light-sensitive film rated at approximately ASA 6000. Photographs of the bubble streaklines were typically taken at shutter speeds ranging from 1/60 to 1/4 s. Rhode[4] describes at length the flow visualization studies. Three different techniques are used, including neutrally buoyant helium-filled soap bubbles[11] using a Sage Action, Inc., bubble generator,[12] smoke-wire,[13-15] and tufts.[16,17]

D. Mean Velocity Measurement

Many instruments are used for separately measuring the magnitude and direction of fluid velocity.[18] However, there are only a few instruments capable of simultaneously sensing both magnitude and direction. One of the simplest of these is the five-hole pitot probe which has been developed and used by various investigators.[19-22] The particular probe employed in this study is model DC-125-12-CD from United Sensor and Control Corp. It is shown schematically in Fig. 3 and has a 3.2-mm-diam sensing tip and shaft containing five tubes. The sensing head is hook-shaped to allow probe shaft rotation without altering the probe tip location.

The instrumentation system, in addition to the five-hole pitot probe, consists of a manual traverse mechanism, two five-way ball valves, a very sensitive pressure transducer, a power supply, and an integrating voltmeter. The differential pressure transducer is model 590D from Datametrics, Inc. The output is read as the dc signal from a TSI model 1076 integrating voltmeter.

Prior to production measurements, the five-hole pitot probe is aerodynamically zeroed for yaw, which is in the horizontal plane of Fig. 4, so that x and θ axes of the measurement coordinate frame coincide with those of the test section. The measurement procedure for each location within a traverse begins with aerodynamically nulling the yaw, and determining the yaw angle β. This is indicated by a zero reading for $p_W - p_E$, where the pressures are identified in Fig.

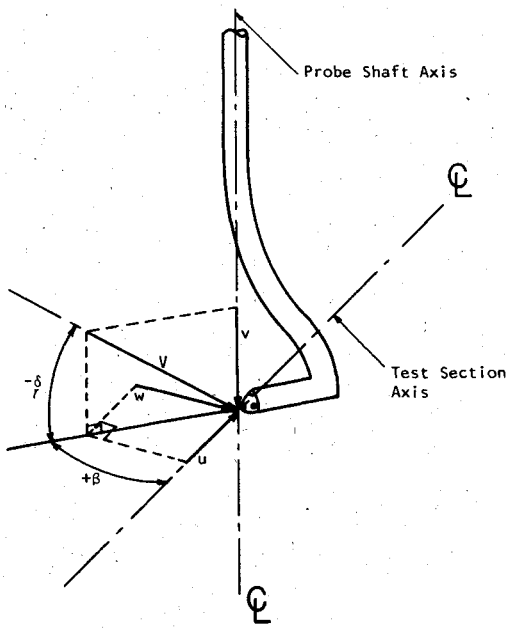

Fig. 4 Velocity components and flow direction angles associated with five-hole pitot measurements (yaw angle β in the horizontal plane and pitch angle δ in the vertical plane).

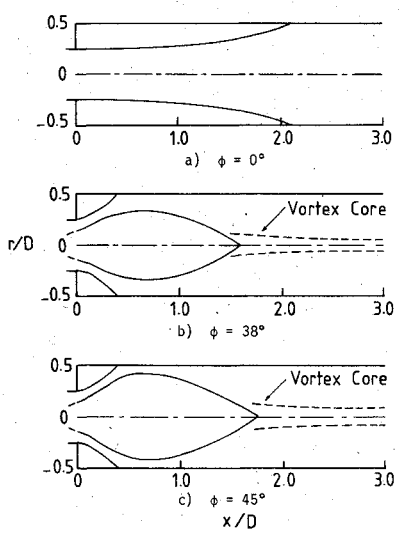

Fig. 5 Artistic impressions of dividing streamlines with wall expansion angle $\alpha = 90$ deg for swirl vane angles.

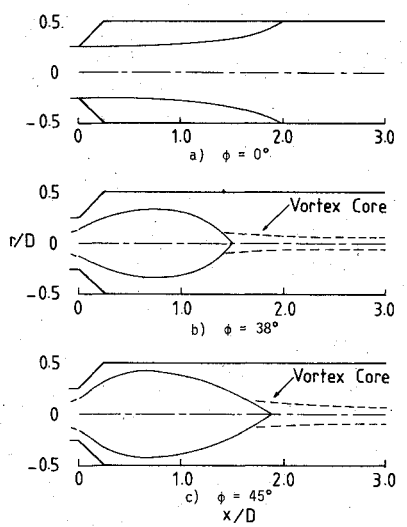

Fig. 6 Artistic impressions of dividing streamlines with wall expansion angle $\alpha = 45$ deg for swirl vane angles.

3. Then the five-way switching valves are set so that $p_N - p_S$ is sensed by the transducer. Finally, the reading of $p_C - p_W$ is similarly obtained.

The data reduction employs two calibration curves which were obtained from a single calibration velocity. The underlying principle is that the calibration is independent of probe Reynolds number Re_p based on probe tip diameter. Careful calibration experiments reveal that this condition exists for $Re_p \geq 1090$ corresponding to a local velocity of 5.4 m/s. Hence measurements of such low velocities suffer from a necessary calibration error. However, this error affects the velocity measurements typically by less than 6% for $Re_p \geq 400$, corresponding to a local velocity greater than 2 m/s.

The data at each measurement location are reduced using a computer program by first calculating the pitch coefficient $(p_N - p_S)/(p_C - p_W)$. From these values an interpolation technique is used to obtain the pitch angle δ in the vertical plane from the appropriate calibration characteristic. The resulting value of δ is utilized to determine the velocity coefficient $\rho V^2/[2(p_C - p_W)]$ using the corresponding calibration characteristic.

Values for V as well as the axial, radial, and swirl velocity components u, v, and w, shown in Fig. 4, are calculated from the velocity coefficient, pitch angle δ, and yaw angle β, which is in the horizontal plane. The magnitude of the velocity vector is given by

$$V = \left[\frac{2}{\rho}\,\frac{\rho V^2}{2(p_C - p_W)}\,(p_C - p_W)\right]^{1/2}$$

and the velocity components are obtained from this magnitude and the pitch and yaw angles.

Elsewhere, Rhode[4] describes the five-hole pitot probe calibration procedure, which is extremely critical to the accuracy of the results, and discusses reliability, since turbulence effects on pressure probes are not well known.[23] A 5% accuracy is expected for most of the measurements, increasing to 10% in regions of low velocity below approximately 2 m/s because of probe insensitivity to low dynamic pressure. It is further asserted that measurements made at flow Reynolds numbers Re_d (based on inlet pipe diameter) equal to 1.05×10^5 and 7.8×10^4 for the nonswirling and swirling flows, respectively, are in the Reynolds number invariant regime.

III. Flow Visualization

Recirculation zones are important to combustor designers. The size and location of these regions in the present isothermal flows are deduced from flow visualization photographs of tufts, smoke, and bubbles responding to the experimental flowfield patterns. Resulting dividing streamline sketches as well as selected photographs of the visualization experiments are now presented and discussed.

A. Artistic Impressions of Streamline Patterns

Photographs of each of the six flowfields resulting from $\phi = 0$, 38, and 45 deg with $\alpha = 90$ and 45 deg have been examined in detail for each of the three flow visualization methods currently employed. The characteristics of the overall flowfield are illustrated and discussed via the resulting time-mean dividing streamline patterns. These are sketched in Figs. 5 and 6 from information obtained from the entire collection of flow visualization photographs. Results from the smoke-wire experiment are utilized near the inlet, whereas tuft and bubble data are used in approximating the size and shape of the recirculation zones downstream. Also, bubble flow patterns reveal the existence of a precessing vortex core, which occurs downstream of the central region.

The resulting streamlines for the three swirl cases of the sudden expansion $\alpha = 90$-deg geometry are shown in Fig. 5.

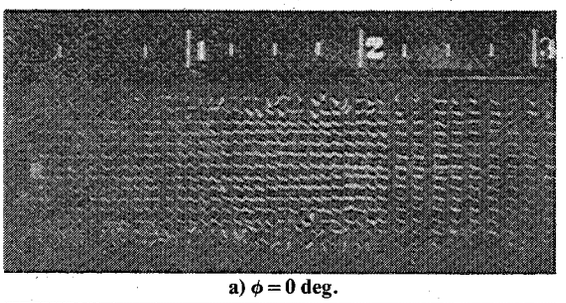

a) $\phi = 0$ deg.

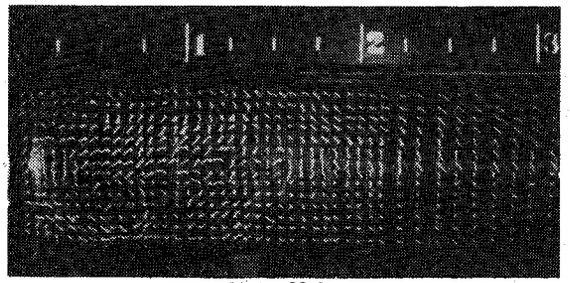

b) $\phi = 38$ deg.

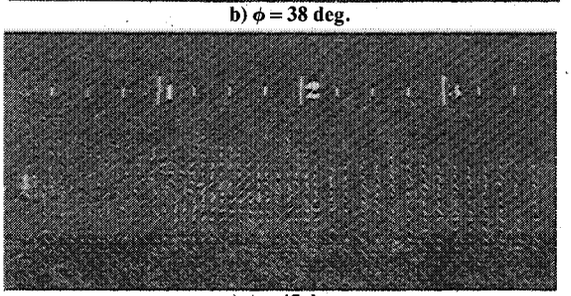

c) $\phi = 45$ deg.

Fig. 7 Flow visualization photographs of tufts in the *rx* plane with wall expansion angle $\alpha = 90$ deg for swirl vane angles.

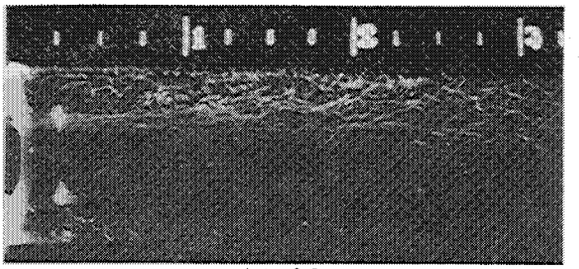

a) $\phi = 0$ deg.

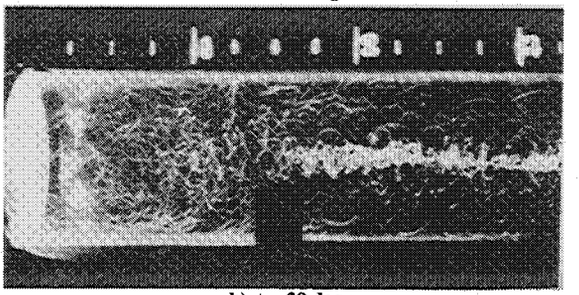

b) $\phi = 38$ deg.

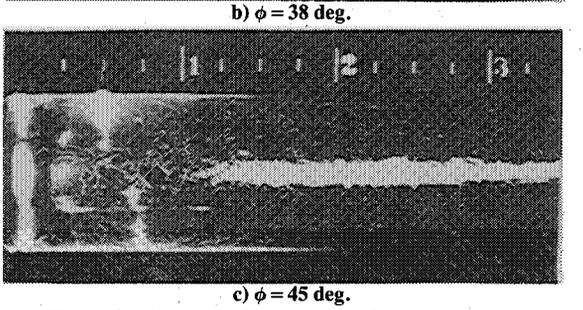

c) $\phi = 45$ deg.

Fig. 9 Flow visualization photographs of pathlines indicated by illuminated neutrally buoyant soap bubbles for wall expansion angle $\alpha = 90$ deg and swirl vane angles.

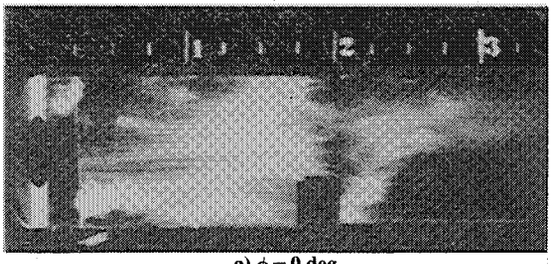

a) $\phi = 0$ deg.

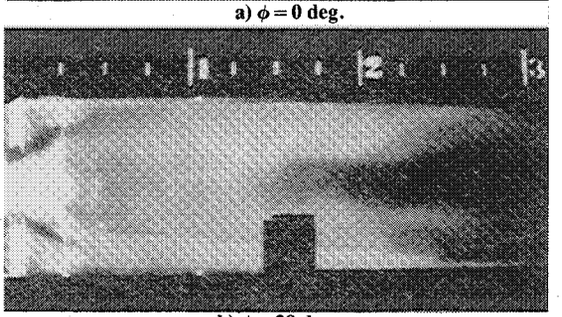

b) $\phi = 38$ deg.

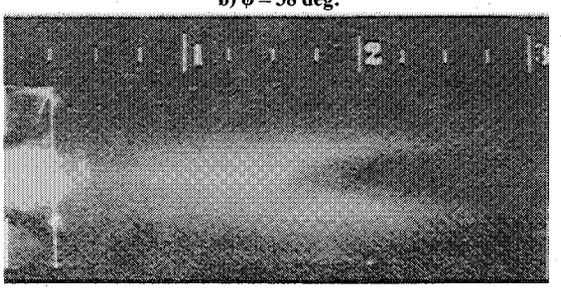

c) $\phi = 45$ deg.

Fig. 8 Flow visualization photographs of smoke-wire streaklines with wall expansion angle $\alpha = 90$ deg for swirl vane angles.

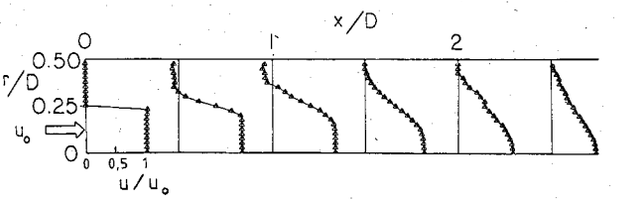

Fig. 10 Measured velocity profiles for wall expansion angle $\phi = 90$ deg and swirl vane angle $\phi = 0$ deg.

The nonswirling flow sketch in Fig. 5a exhibits a large corner recirculation zone which is in excellent agreement with the corresponding streamlines from the measurements of Chaturvedi.[8] Appropriate prior measurements for the present swirling flows have not been found. For the moderate swirl vane angle case of $\phi = 38$ deg a central recirculation region appears in conjunction with a decrease in size of the corner zone. A thin precessing vortex core, discussed at length by Syred and Beer,[24] is observed near the centerline extending from the end of the central region to the test section exit. The axial location where the vortex core begins fluctuates, ranging approximately from $x/D = 1.25$ to 1.75. This vortex core is essentially a three-dimensional time-dependent phenomenon, which occurs as a swirling region of negligible axial velocity whose center winds around the test section centerline. A further increase in vane angle to $\phi = 45$ deg results in slight enlargement of the central zone; however, the corner bubble is essentially unaffected. For this flowfield the vortex core is slightly expanded in the radial direction.

The corresponding sequence of dividing streamlines is found in Fig. 6 for the gradual flow expansion case with $\alpha = 45$ deg. As with Fig. 5, the nonswirling flowfield exhibits excellent agreement with corresponding measurements of

Chaturvedi.[8] No evidence of a corner zone is found from examination of the entire photograph collection for the intermediate vane angle case, although the flow pattern is otherwise very similar to the corresponding flow for $\alpha = 90$ deg. The flowfield with $\phi = 45$ deg produces exactly the same effects as in the abrupt expansion case of Fig. 5.

B. Flow Visualization

Tuft visualization is very important in that it supplies an overall view of local flow direction. As discussed in Sec. II.C, photographs at various shutter speeds were obtained. Slower speeds show more of the temporal behavior, although the tufts are sometimes not distinctly visible in portions of the flowfield. Some of the more noteworthy photographs are presented here, encompassing a range of shutter speeds. Velocities in recirculation zones are often somewhat lower than in other portions of the flowfield, and thus under such conditions there may be insufficient drag on a tuft to align it accurately with the local flow direction. However, this is taken into consideration in interpreting the photographed results.

The three flowfields for $\alpha = 90$ deg are characterized in Fig. 7 as photographs of the rx-screen tufts. Figure 7a identifies the corner zone reattachment point for the nonswirling flowfield. It is found to be approximately at $x/D = 2.0$, wherein tufts showing no air motion are considered stagnation points. Further, an indication of the turbulence level is depicted as the rather slow shutter speed of 1/15 s was used.

For swirl vane angle $\phi = 38$ deg, Fig. 7b is a photograph taken at 1/60 s. The swirl is in the counterclockwise direction when viewed from downstream. There is no evidence of a corner zone and the central region apparently extends to $x/D = 1.5$. Finally, the $\phi = 45$ deg case shown in Fig. 7c exhibits a central region extending downstream as far as approximately $x/D = 1.85$ for 1/125-s shutter speed.

Local details in the nonswirling flowfields are clearly revealed through the visualization of streaklines indicated from the generation of illuminated smoke. In the swirling flow cases, strong mixing diffuses the smoke so that streaklines are not distinguishable. However, under such conditions recirculation zone outlines are visible, especially in the region near the smoke-generation wire. A selected photograph is exhibited and discussed for each of the three abrupt expansion flowfields.

The corner recirculation bubble in the nonswirling case with wall expansion angle $\alpha = 90$ deg is revealed in Fig. 8a using 1/30-s shutter speed. Also, the radial location of the zero velocity point within the upper and lower corner bubble is estimated to be approximately $0.15D$ from the respective walls of the test facility. This agrees with the velocity measurements presented later in Sec. IV.

The moderate swirl vane angle flow with a 1/30-s exposure is shown in Fig. 8b. The shortened corner zone is easily identified because the adjacent flow contains no smoke near the inlet. This bubble is seen to extend to approximately $x/D = 0.45$. The tuft photographs for this case indicate a slightly shorter zone ending at approximately $x/D = 0.4$. The upstream portion of the central zone is also clearly seen, as low velocity fluid carries a dense mass of smoke which slowly moves upstream of the inlet. Further, the precessing vortex core is seen to contain only slight smoke. Since the core exhibits negligible axial velocity, the smoke is essentially carried around it by the high velocity fluid outside the core.

Figure 8c is a photograph at 1/8-s of the $\phi = 45$ deg case wherein this core is not as distinct. In this case, some smoke has diffused into the core due to a slightly longer delay before activating the camera shutter. Observe that both the corner and central zones near the inlet reveal that the only change from those for $\phi = 38$ deg is a slightly wider central region.

Soap bubbles injected into the flow upstream of the test section trace pathlines clearly when illuminated. In relatively lower turbulence intensity portions of the flowfield mean-flow directions can be obtained by ensemble averaging local tangents to pathlines traced out by soap bubbles. This helps define the flowfield geometry in terms of the outline of recirculation regions.

A sample flow visualization photograph is presented in Fig. 9a corresponding to the zero swirl, 90-deg expansion angle flowfield. The photograph, taken with a relatively long time exposure (1/8-s), clearly shows a great number of individual pathlines. Photographs of this type can be used to indicate regions of weakly turbulent flow such as that near the centerline of the flowfield which exhibits relatively straight pathlines. In addition, the outline of the corner recirculation region can be estimated from Fig. 9a (and numerous additional photographs taken at the identical run condition). For this geometry the mean stagnation point defining the end of the recirculation zone appears to be at $x/D = 2.0$.

A photograph with $\phi = 38$ deg and 1/8-s shutter speed is shown in Fig. 9b, where the precessing vortex core is clearly seen extending from $x/D = 1.5$ to the exit. Its upstream extent fluctuates randomly from approximately $x/D = 1.25$ to 1.75. The corner bubble is observed in both the upper and lower portions of the flowfield, extending to approximately $x/D = 0.4$, which agrees almost exactly with the smoke flow pattern for this flowfield in Fig. 8b. A photograph using 1/8-s shutter speed is presented in Fig. 9c for the $\phi = 45$ deg flowfield where a thicker vortex core is seen. The corner zone is faintly visible here, and its axial length also seems to extend to about $x/D = 0.4$.

C. Parametric Effects

Streamline plots allow recirculation zones to be characterized parametrically for the effects of α and ϕ on the corner and central recirculation zone lengths. Several observations should be noted. First, zone lengths are only slightly affected by α, as found previously for the corner bubble under isothermal nonswirling conditions.[8,25] Note that, at these high Reynolds numbers, the corner region length is independent of Reynolds number.[26,27] Second, as side-wall angle α decreases from 90 to 45 deg, the zone lengths typically decrease slightly and the inlet flow is encouraged to impinge on the confining walls. Third, the corner recirculation length decreases upon increasing the swirl vane angle ϕ from 0 to 38 deg, a parameter change which also provokes the existence of a central recirculation bubble and precessing vortex core. Increasing the vane angle further only slightly enlarges the central zone and the vortex core.

IV. Velocity Measurements

A. Sudden Expansion, $\alpha = 90$ deg

Figures 10-12 show the axial and swirl time-mean velocity profiles, for swirl vane angles $\phi = 0$, 38, and 45 deg with a sudden expansion (side-wall angle $\alpha = 90$ deg). Measurements are obtained with the five-hole pitot probe in the manner discussed in Sec. II.D. Note that in these and subsequent figures, different scales are used for the normalized axial and swirl velocities. Radial velocities are consistently much smaller than the axial and swirl components, and they may be inferred from the dividing streamline patterns deduced from flow visualization experiments depicted in Figs. 5 and 6. They need not be presented here. Figure 10 shows the corner recirculation region for the nonswirling flow on the verge of reattachment near $x/D = 2.0$. The corresponding visualization results shown in Fig. 5a give this location as $x/D = 2.1$ and the corresponding measurements of Chaturvedi[8] give a value of $x/D = 2.3$.

In the absence of pertinent measurements, previous predictions of gas turbine combustor flowfields[2,3,28,29] employed an approximation for inlet velocity boundary conditions. It has generally been assumed that $v = 0$ and that both u and w exhibit flat velocity profiles. However, the present

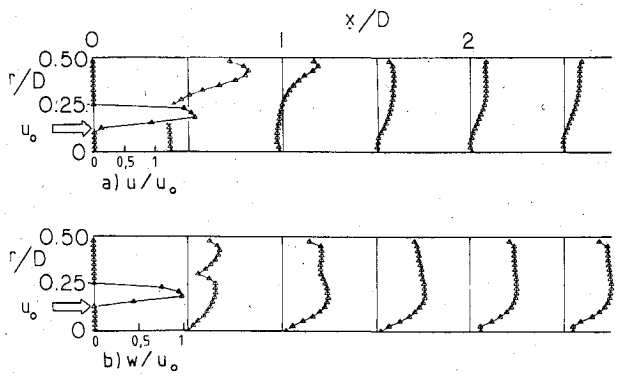

Fig. 11 Measured velocity profiles for wall expansion angle $\phi = 90$ deg and swirl vane angle $\phi = 38$ deg.

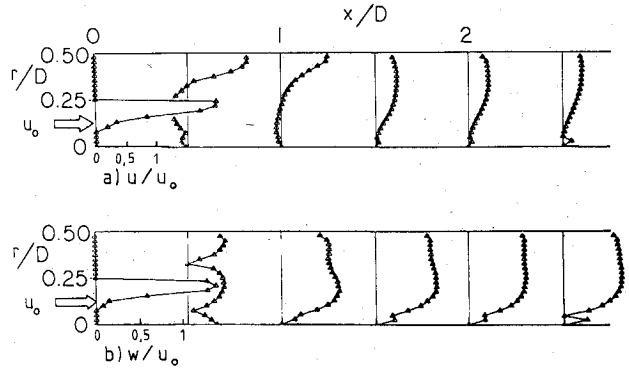

Fig. 12 Measured velocity profiles for wall expansion angle $\alpha = 90$ deg and swirl vane angle $\phi = 45$ deg.

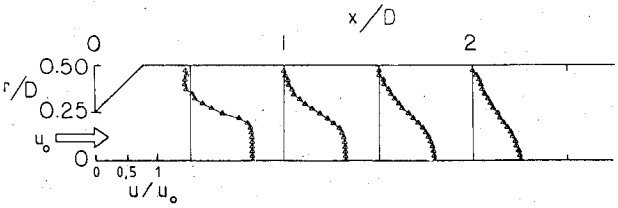

Fig. 13 Measured velocity profiles for wall expansion angle $\alpha = 45$ deg and swirl vane angle $\phi = 0$ deg.

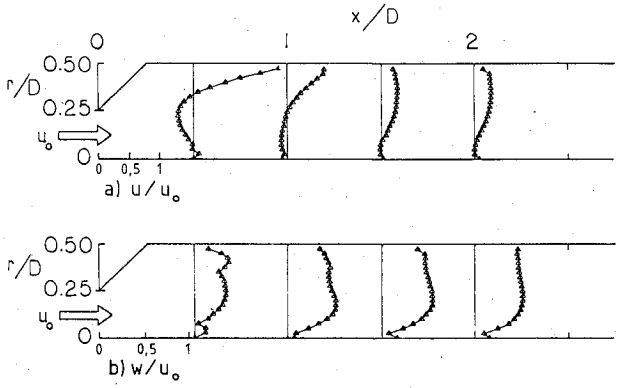

Fig. 14 Measured velocity profiles for wall expansion angle $\alpha = 45$ deg and swirl vane angle $\phi = 38$ deg.

measurements, taken 4 cm downstream of the vane swirler, indicate that this is an unrealistic estimate, with sharply peaked u and w profiles, as shown in Figs. 11 and 12. The difference results from the use of a swirler with ten flat blades with pitch/chord ratio of unity, imperfect blade efficiency, the existence of a hub, and the fact that the downstream edge of swirl vanes of the test facility is actually located ap-

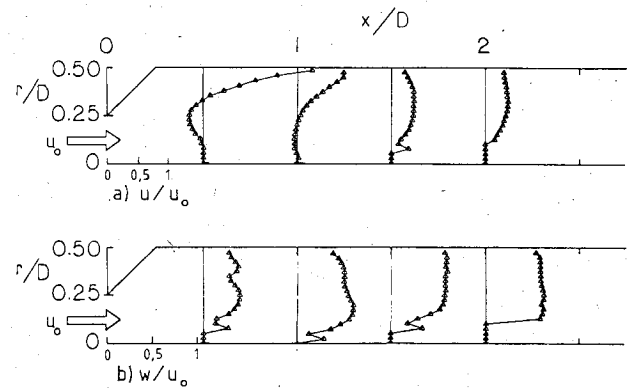

Fig. 15 Measured velocity profiles for wall expansion angle $\alpha = 45$ deg and swirl vane angle $\phi = 45$ deg.

proximately 4 cm upstream of the flow expansion corner, where $x/D = 0$. This swirler location allows the central recirculation zone to begin upstream of $x/D = 0$, thereby changing the velocity profiles there.

Figure 11 also reveals that a 38-deg swirl vane angle produces a maximum swirl flow angle [$\tan^{-1}(w_o/u_o)$] of 30 deg at the test chamber inlet. The maximum swirl flow angle for the 45-deg vane angle case shown in Fig. 12 is 34 deg. Thus there is only a slight increase of swirl flow angle, although these two flows are different in that the inlet profiles are considerably more sharply peaked for the latter case. Figures 11 and 12 show zero u and w velocity values near the axis at the inlet, but actually the probe was insensitive to the very low velocities there. This is consistent with earlier flow visualization results that the central bubble extends upstream of the inlet. The measurements shown in Fig. 11a provide no evidence regarding the existence of a corner zone. This is expected because flow visualization reveals that the region only extends to $x/D = 0.4$. However, there is clear evidence of a rather large central zone whose length is similar to that shown in Fig. 5b. Although the axial velocity profiles are beginning to flatten in the downstream direction, they retain a zero velocity value on the axis, which is consistent with soap bubble flow patterns as seen in Fig. 9b. The early erratic behavior shown by the swirl velocity profiles in Fig. 11b quickly transforms, exhibiting a solid-body-rotation core with a rather flat profile outside this region.

Figure 12 also reveals the discrepancy regarding inlet velocity profiles, this time for the case $\phi = 45$ deg. The large central recirculation region causes the downstream flow to be accelerated near the top wall. The corresponding swirl velocity component at the $x/D = 0.5$ axial station typically shows local minima where the mean axial velocity is zero. The accuracy of the velocity measurements at these locations is poor, as discussed in Sec. II.D, so that any physical interpretation here is suspect. Again, the early erratic behavior found in the swirl velocity profile at $x/D = 0.5$ quickly develops into a shape similar to that seen in Fig. 11b. The precessing vortex core motion discussed in Sec. II.B results in poor measurement repeatability which promotes the irregular behavior within this core region.

B. Gradual Expansion, $\alpha = 45$ deg

Figures 13-15 exhibit velocities for the same sequence of flowfields with side-wall angle $\alpha = 45$ deg. The inlet profiles were not measured in this geometry because the presence of the expansion block interferes with probe positioning. Effects of swirl vane angle ϕ on velocities, similar to those found for the sudden expansion cases, are found in the flowfield sequence for this test section geometry. The major difference is that the sloping wall encourages the inlet flow to accelerate near the top wall. Also, it tends to shorten or obliterate the corner recirculation region.

C. Comparison of Measurements and Predictions

Flowfield computations have been made[2-4] for a variety of side-wall and swirl vane angles, using the standard k-ϵ turbulence model and the technique discussed at length elsewhere.[30] These and other earlier predictions have generally idealized the inlet flow as a plug-flow axial velocity profile with a flat or solid body rotation swirl velocity profile. Though this may be adequate for those applications, it is clearly inadequate for the present study, in which the inlet flow conditions are highly nonuniform. Current work is proceeding with inlet profile effects and turbulence model developments. In this connection, it may be noted that a turbulence model whose basis and parameters are adequate for simple flow situations is not adequate to handle the more complicated swirling recirculating flow situation. Nevertheless, good predictions are available[4] for the case of a less difficult test problem (coswirl and counterswirl flow in a pipe using the data of Ref. 31). This turbulence simulation problem in complex flowfields is clearly an area of current research interest.

V. Summary

A major outcome of the current study is the experimental characterization of corner and central recirculation zones in six basic flowfield configurations of an axisymmetric expansion with side-wall angle $\alpha = 90$ and 45 deg and swirl vane angle $\phi = 0$, 38, and 45 deg. The size and shape of the recirculation bubbles for each flowfield is illustrated via an artistic impression deduced from a collection of flow visualization photographs of tufts, smoke, and neutrally buoyant soap bubbles responding to the flow. Increasing swirl vane angle ϕ from 0 to 38 deg produces a shortened corner region and the appearance of a central bubble typically extending downstream to approximately $x/D = 1.7$, after which a precessing vortex core exists near the axis reaching to the exit of the test section. A further increase in ϕ to 45 deg enlarges the central zone and vortex core with negligible effect on the corner region in those flowfields where it occurs. The effect of side-wall angle α on the nonswirling flows is negligible. However, a decrease from 90 to 45 deg apparently eliminates the corner bubble in the swirling flow cases investigated. This decrease in α also causes the inlet flow to impinge more severely on the top wall, where larger axial velocities occur.

A more detailed experiment consists of the measurement of time-mean velocity components in the axial, radial, and azimuthal directions using a five-hole pitot probe. These measurements generally agree with the flow visualization results and provide a more complete understanding of each flowfield. At the inlet, the axial and swirl velocity profiles exhibit maximum values at approximately $r/D = 0.2$ in a sharply peaked annular fashion. This nonuniformity arises for several reasons: the use of a ten-blade swirler with pitch/chord ratio of 1, blade inefficiency, the presence of a hub, and the fact that the swirl vane exit station is typically located upstream of the expansion station. This allows the central recirculation zone to begin upstream of the expansion where $x/D = 0$.

Clearly, the time-mean velocity measurements presented here contribute to a seriously needed data base for the validation of computer prediction codes and the development of turbulence models for the simulation of complex turbulent swirling flows.

Acknowledgments

The authors wish to express their sincere gratitude to NASA Lewis Research Center and Air Force Wright Aeronautical Laboratories for support under Grant NAG 3-74.

References

[1] Lefebvre, A.H., ed., *Gas Turbine Combustor Design Problems*, Hemisphere-McGraw-Hill, New York, 1980.

[2] Rhode, D.L., Lilley, D.G., and McLaughlin, D.K., "On the Prediction of Swirling Flowfields Found in Axisymmetric Combustor Geometries," *Proceedings of ASME Symposium on Fluid Mechanics of Combustion Systems*, Boulder, Colo., June 1981, pp. 257-266; see also *Journal of Fluids Engineering*, Vol. 104, Sept. 1982, pp. 378-384.

[3] Lilley, D.G., Rhode, D.L., and Samples, J.W., "Prediction of Swirling Reacting Flow in Ramjet Combustors," AIAA Paper 81-1485, July 1981.

[4] Rhode, D.L., *Predictions and Measurements of Isothermal Flowfields in Axisymmetric Combustor Geometries*, Ph.D. Thesis, Oklahoma State Univ., Stillwater, Okla., Dec. 1981.

[5] Habib, M.A. and Whitelaw, J.H., "Velocity Characteristics of Confined Coaxial Jets With and Without Swirl," ASME Paper 79-WA/FE-21, Dec. 1979.

[6] Srinivasan, R. and Mongia, H.C., "Numerical Computations of Swirling Recirculating Flows," Final Report, NASA-CR-165196, Sept. 1980.

[7] Sturgess, G.J., Syed, S.A., and Sepulveda, D., "Application of Numerical Modeling to Gas Turbine Combustor Development Problems," *Proceedings of ASME Symposium on Fluid Mechanics of Combustion Systems*, Boulder, Colo., June 1981, pp. 241-250.

[8] Chaturvedi, M.C., "Flow Characteristics of Axisymmetric Expansions," *Proceedings of the Journal of Hydraulics Division*, ASCE, Vol. 89, HY3, 1963, pp. 61-92.

[9] Gosman, A.D., and Pun, W.M., "Calculation of Recirculating Flows," Report HTS/74/2, Dept. of Mechanical Engineering, Imperial College, London, England, 1974.

[10] Morel, T., "Comprehensive Design of Axisymmetric Wind Tunnel Contractions," ASME Paper 75-FE-17, Minneapolis, Minn. May 1975.

[11] Owen, F.S., Hale, R.W., Johnson, B.V., and Travers, A., "Experimental Investigation of Characteristics of Confined Jet-Driven Vortex Flows," United Aircraft Research Laboratories, East Hartford, Conn., Rept. R-2494-2, Nov. 1961.

[12] Hale, R.W., Tan, P., Stowell, R.C. and Ordway, D.E., "Development of an Integrated System for Flow Visualization in Air Using Neutrally-Buoyant Bubbles," Sage Action, Inc., Ithaca, N.Y., for ONR, Rept. SAI-RR 7107, Dec. 1971.

[13] Corke, T., Koga, D., Drubka, R., and Nagib, H., "A New Technique for Introducing Controlled Sheets of Smoke Streaklines in Wind Tunnels," *Proceedings of International Congress on Instrumentation in Aerospace Simulation Facilities*, IEEE Publ. 77 CH 1251-8 AES, 1974, p. 74.

[14] Nagib, H.M., "Visualization of Turbulent and Complex Flows Using Controlled Sheets of Smoke Streaklines," *Proceedings of International Symposium on Flow Visualization*, Tokyo, Oct. 1977, pp. 181-186; see also Supplement, pp. 29-1 to 29-7.

[15] Cornell, D., "Smoke Generation for Flow Visualization," Aerophysics Research Report 54, Mississippi State Univ., University, Miss., Nov. 1964.

[16] Bird, J.D., "Visualization of Flowfields by Use of a Tuft Grid Technique," *Journal of the Aeronautical Sciences*, Vol. 19, 1952, pp. 481-485.

[17] McMahon, H.M., Hester, D.D., and Palfery, J.G., "Vortex Shedding From a Turbulent Jet in a Cross-Wind," *Journal of Fluid Mechanics*, Vol. 48, 1971, pp. 73-80.

[18] Breyer, D.W. and Pankhurst, R.C., "Pressure-Probe Methods for Determining Wind Speed and Flow Direction," Her Majesty's Stationery Office, London, England, 1971.

[19] Hiett, G.F. and Powell, G.E., "Three-Dimensional Probe for Investigation of Flow Patterns," *The Engineer*, Vol. 213, Jan. 1962, pp. 165-170.

[20] Pien, P.C., "The Five-Hole Spherical Pitot Tube," David Taylor Model Basin Report 1229, May 1958.

[21] Lee, J.C. and Ash, J.B., "A Three-Dimensional Spherical Pitot Probe," *Transactions of ASME, Journal of Applied Mechanics*, Vol. 23, April 1956, pp. 603-608.

[22] Hale, M.R. and Norrie, D.H., "The Analysis and Calibration of the Five-Hole Spherical Pitot," ASME Paper 67-WA/FE-24, Nov. 1967.

[23] Gupta, A.K. and Lilley, D.G., *Flowfield Modeling and Diagnostics*, Abacus Press, Tunbridge Wells, Kent, England, 1983 (in press).

[24] Syred, N. and Beer, J.M., "Combustion in Swirling Flows: A Review," *Combustion and Flame*, Vol. 23, 1974, pp. 143-201.

[25] Lipstein, N.J., "Low Velocity Sudden Expansion Pipe Flow," Paper presented at ASHRAE 69th Annual Meeting, Miami Beach, Fla., June 1962.

[26] Pratte, B.D. and Keffer, J.R., "The Swirling Turbulent Jet," *Transactions of ASME, Journal of Basic Engineering*, Vol. 94, Dec. 1972, pp. 739-748.

[27] Syred, N. and Dahman, K.R., "Effect of High Levels of Confinement Upon the Aerodynamics of Swirl Burners," *Journal of Energy*, Vol. 2, Jan.-Feb. 1978, pp. 8-15.

[28] Novick, A.S., Miles, G.A., and Lilley, D.G., "Numerical Simulation of Combustor Flowfields," *Journal of Energy*, Vol. 3, March-April 1979, pp. 95-105.

[29] Serag-Eldin, M.A. and Spalding, D.B., "Computations of Three-Dimensional Gas Turbine Combustion Chamber Flows," *Transactions of ASME, Journal of Engineering for Power*, Vol. 101, July 1979, pp. 326-336.

[30] Lilley, D.G. and Rhode, D.L., "A Computer Code for Swirling Turbulent Axisymmetric Recirculating Flows in Practical Isothermal Combustor Geometries," NASA CR-3442, Feb. 1982.

[31] Vu, B.T. and Gouldin, F.C., "Flow Measurements in a Model Swirl Combustor," *AIAA Journal*, Vol. 20, May 1982, pp. 642-651.